Tipping Point for Expansion of Layered Aluminosilicates in Weakly Polar Solvents: Supercritical CO2

Herbert T. Schaef[1]*, Narasimhan Loganathan[2], Geoffrey M. Bowers[3], R. James Kirkpatrick[2], A. Ozgur Yazaydin[2,4], Sarah D. Burton[5], David W. Hoyt[5], K. Sahan Thanthiriwatte[6], David A. Dixon[6], B. Peter McGrail[1], Kevin M. Rosso[1], Eugene S. Ilton[1]*, John S. Loring[1]*

[1]Pacific Northwest National Laboratory, Richland WA 99356

[2]College of Natural Science, Michigan State University, East Lansing, MI, 48824

[3]Department of Chemistry and Biochemistry, St. Mary's College of Maryland, St. Mary's City, MD 20686

[4] Department of Chemical Engineering, University College London, London, WC1E 7JE, United Kingdom

[5]William R. Wiley Environmental and Molecular Sciences Laboratory, Pacific Northwest National Laboratory, Richland, WA, 99356

[6]Department of Chemistry, The University of Alabama, Tuscaloosa, AL 35487

KEYWORDS: carbon dioxide; montmorillonite; intercalation: Molecular dynamics; interlayer expansion.

ABSTRACT: Layered aluminosilicates play a dominant role in the mechanical and gas storage properties of the subsurface, are used in diverse industrial applications, and serve as model materials for understanding solvent-ion-support systems. Although expansion in the presence of H_2O is well known to be systematically correlated with the hydration free energy of the interlayer cation, in environments dominated by non-polar solvents (i.e. CO_2), uptake into the interlayer is not well-understood. Using novel high pressure capabilities, we investigated the interaction of dry supercritical CO_2 with Na^+-, NH_4^+-, and Cs^+-saturated montmorillonite, comparing results with predictions from molecular dynamics simulations. Despite the known trend in H_2O, and that cation solvation energies in CO_2 suggest a stronger interaction with Na^+, both the NH_4^+- and Cs^+-clays readily absorbed CO_2 and expanded while the Na^+-clay did not. The apparent inertness of the Na^+-clay was not due to kinetics, as experiments seeking a stable expanded state showed that none exists. Molecular dynamics simulations revealed a large endothermicity to CO_2 intercalation in the Na^+-clay, but little or no energy barrier for the NH_4^+- and Cs^+-clays. Indeed, the combination of experiment and theory clearly demonstrate that CO_2 intercalation of Na-montmorillonite clays is prohibited in the absence of H_2O. Consequently, we have shown for the first time that in the presence of a low dielectric constant gas swelling depends more on the strength of the interaction between interlayer cation and aluminosilicate sheets and less on that with solvent. The finding suggests a distinct regime in layered aluminosilicates swelling behavior triggered by low solvent polarizability, with important implications in geomechanics, storage and retention of volatile gases, and across industrial uses in gelling, decoloring, heterogeneous catalysis, and semi-permeable reactive barriers.

INTRODUCTION

Layered aluminosilicates have unique properties that emerge from their quasi-2D structure, composition, permanent layer charge, and charge-balancing interlayer cations. As a primary source of nanoporosity[1-2] gas absorptivity[3-4], and ductility[5] in sedimentary rocks, their specific behavior, even in small concentrations, can control the geomechanical response of caprocks that seal reservoir formations[6] or the extraction of natural gas from organic rich shales that are the source rocks driving the present fracking boom.[7] They are also used widely in industrial applications that range from catalytic substrates[8] to metal and gas sorbents[9-10] to reactive barrier materials.[11]

A key characteristic is their ability to expand or contract by absorbing or ejecting solvent and ions in response to changing fluid chemistry.[12] Layered aluminosilicates known as smectites are of particular interest, because they can swell substantially in the presence of certain volatiles[13-14] due to incorporation of these species in their interlayer galleries. The extent to which swelling will be significantly altered when exposed to fracking fluids during gas extraction from shales and supercritical CO_2 ($scCO_2$) during and after injection of CO_2 into geologic reservoirs is often a crucial unknown.[15] Unlike swelling performance requirements for clay based barriers in nuclear repositories[16], geologic exploration operations using non-aqueous based technologies (i.e. $scCO_2$) are

designed to avoid clay swelling[17] to minimize threats to formation permeability.

Solvent selectivity in smectite swelling is not comprehensively well understood; while their swelling behavior when exposed to H_2O is well known[18-20], in multiphase and non-aqueous fluids questions remain regarding the underlying forces that lead to solvent uptake and expansion of the interlayer region. With respect to H_2O, the degree of H_2O intercalation and induced swelling largely depends on the hydration free energy of the interlayer cation.[21-22] This is best demonstrated by comparing swelling behaviors of Na^+ montmorillonites[19], which maintain two layers of hydration (2W) to the identical clay containing Cs^+, a so-called swelling hindrance interlayer cation, that restrict hydration to a 1W state.[21] With respect to weakly polar solvents such as CO_2, recent laboratory studies have clearly demonstrated reversible volumetric transformations of smectite minerals due to exposure to gaseous CO_2 ($CO_{2(g)}$) or $scCO_2$.[13, 23-30] For example, a number of studies[13, 28] have reported increased basal spacings when montmorillonite with less than a full layer of H_2O molecules (sub 1W) was exposed to $scCO_2$, evidence that CO_2 enters the interlayer at least under relatively low H_2O chemical potentials. A striking observation was that H_2O and CO_2 intercalation was both synergistic and competitive: fully collapsed Na-montmorillonite neither expanded nor sorbed CO_2 into the interlayer region when exposed to dry $scCO_2$.[26, 31-33] However, small additions of H_2O to $scCO_2$ promoted CO_2 intercalation up to a critical H_2O concentration beyond which H_2O expelled CO_2 from the interlayer region. An intuitive explanation is that because the free energy of solvation for H_2O-Na^+ in the interlayer is expectedly larger than that for Na-CO_2, even at relatively low H_2O concentrations hydrated or partially hydrated Na^+ essentially props the interlayers open, allowing CO_2 to enter as secondary outcome. Indeed, calculated solvation energies for Na^+ in bulk water and $scCO_2$[34] show that the solvation energies for Na^+ in $scCO_2$ are ~50% less than for Na^+ in water. What is missing from such observations is a fundamental understanding of the behavior of the system in the complete absence of water. In other words, can nonpolar solvents, which do not have as strong an interaction with interlayer cations, drive open the interlayer space and, if so, why and under what conditions? A cation solvation-based interpretation alone ignores the importance of cation interaction with the aluminosilicate framework.

Probing the interactions of CO_2, interlayer cations, and the aluminosilicate structural units within nano-crystallites, a common size range for these minerals, is challenging. Confinement in the nanometer-scale interlayer space may alter the equilibrium configurations of relevant species. Theoretical studies have provided some insight into energetic barriers to intercalation, solvation of interlayer cations by CO_2, as well as the thermomechanical properties of clays.[35-42] Calculations by Makaremi et al.[40], in the absence of H_2O, suggest a large energy barrier for CO_2 intercalation into a fully collapsed Na-montmorillonite at both supercritical and non-supercritical conditions. The results also show that an expanded state near $d(001)$ = ~12.3 Å is metastable. The presence of an energy barrier to CO_2 intercalation is consistent with the experiments discussed above. Whether a stable expanded state for Na-montmorillonite/CO_2 exists or not has never been determined experimentally.

Enabled by novel *in situ* capabilities, here we explore the balance between cation-aluminosilicate and cation-CO_2 interactions with respect to CO_2 intercalation and swelling. We vary interlayer monovalent cation radius by using Na^+, NH_4^+, and Cs^+ to systematically tune the strength of the interaction with the aluminosilicate sheet and their solvation free energies with CO_2. Similar to H_2O-cation interactions, classical molecular dynamics (MD)[34] and high-level *ab initio* calculations (**Figure 1**) suggest that CO_2-cation solvation energies decrease in magnitude with increasing cation size (or charge density) from Na^+ → Cs^+. However, the solvation energies for CO_2-cation are on the order of 50% lower than for H_2O. Consequently, we hypothesize that the relatively low CO_2-cation solvation energies will highlight the interaction of the interlayer cation with the aluminosilicate structural units. Three dry montmorillonites (Na^+, NH_4^+, or Cs^+ saturated SWy-2) were reacted with anhydrous $scCO_2$ and characterized in detail *in situ*. If the clays with the larger cations (NH_4^+ or Cs^+) expand but Na-clay does not, then the expansion cannot be attributed to the strength of the solvent interaction with the interlayer cation but rather the strength of the cation interaction with aluminosilicate sheet surfaces. However, this observation would not unambiguously identify the cause of CO_2 intercalation per se, because the propping effect of larger cations conceptually can enhance CO_2 diffusivity and uptake.[45] We directly test this by performing experiments that evaluate if the clay remains expanded or collapses once the "props" are removed, thus constraining the possible existence of a stable expanded state for the Na-montmorillonite/CO_2 system. Modifications to the clay structure were probed with x-ray diffraction (XRD), while changes in the CO_2 chemical environment were analyzed using infrared (IR) spectroscopy. Perturbations in the CO_2 molecules in the interlayer, including information on CO_2-cation interaction, were analyzed by magic angle spinning nuclear magnetic resonance (MAS-NMR) spectroscopy. All measurements were performed on the fluid/clay system in situ under controlled pressurized conditions. Molecular dynamics simulations at the same conditions using the Grand Canonical ensemble (GCMD) were used to map the free energy landscape as a function of CO_2 intercalation and interlayer spacing for model Na^+, NH_4^+, and Cs^+ clay structures. Collectively, in contrast to swelling behavior in H_2O systems, our findings demonstrate that cation-clay interactions play the commanding role relative to solvation of interlayer cations for clay expansion in weakly to non-polar solvents such as CO_2.

RESULTS AND DISCUSSION

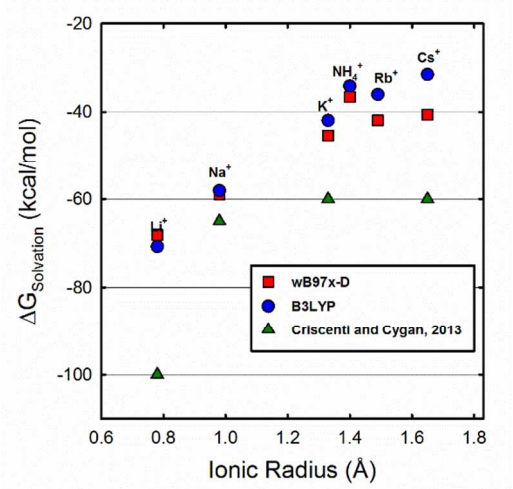

Figure 1. Free energy of solvation by CO_2 versus ionic radius[43-44] for alkali cations and the ammonium cation calculated using electronic structure calculations (see supplemental information). Also shown are values calculated by Criscenti and Cygan et al.,[34] using classical molecular dynamics simulations.

Pressurized X-ray Diffraction

The *d*(001) values of SWy-2 (Na^+, Cs^+, and NH_4^+) were determined by XRD at atmospheric (24°C and ~35% RH) and vacuum (~10^{-3} Torr, 50°C) conditions, and during exposure to CO_2 at 90 bar (50°C). The measured peak centroids of the d(*001*) basal reflections are listed in **Table 1** (see **Figure S1** for the XRD tracings). The range of values for *d*(001) under atmospheric conditions (~35% RH) are consistent with those reported in the literature for nominally the same clays and similar conditions.[18, 46-48]

The *d*(001) values for all the clays decreased when exposed to vacuum (10^{-3} Torr, 50°C), indicating the removal of interlayer water. The *d*(001) value (9.75Å) for Na-SWy-2 is slightly larger than the reported value (9.66 Å) for a completely dehydrated Na-SWy-1;[19] where the Na^+ cations are coordinated by six basal oxygen atoms.[46, 49] The larger *d*(001) value (11.13 Å) for Cs-SWy-2 correlates with the relatively larger size of the Cs^+ cation (Cs: 1.69 Å, Na:0.95 Å , and NH_4:1.43 Å)[50-51] . Calculated and experimental *d*(001) values from the literature show a significant range for dehydrated Cs-montmorillonite. For example, Bérend et al.,[18] cite values from 10.7 to 11.35 Å; their own experimental work on Cs-SWy-1 yielded *d*(001) = 11.08 Å (exposed to vacuum at 100 °C for 4-24 hours). Simulations of anhydrous Cs^+ smectites consistently yield smaller *d*(001) values compared to experiment, with spacings ranging from 10.50 to 10.70 Å. [48, 52-53] The *d*(001) values for NH_4-SWy-2 reported here are intermediate (10.39-10.49 Å) with respect to the Na^+ and Cs^+ clays. Gautier et al.[47] also analyzed an anhydrous NH_4-SWy-2 sample and reported *d*(001) = ~10.4 Å, consistent with the present study.[54]

Both Cs^+ and NH_4^+ montmorillonite expanded during exposure to $scCO_2$, but Na^+ montmorillonite did not (**Table 1**). Other than peak intensity attenuation from the dense CO_2 fluid, the patterns for Na^+ montmorillonite were essentially identical under vacuum and exposure to $scCO_2$ (see **Figure S1-S3**). When the pressurized experiments were opened to the vacuum for a few minutes, the Cs^+ and NH_4^+ clays collapsed back to their original vacuum basal spacing with no sign of alteration or secondary phase formation.

Table 1. Measured and [calculated] *d*(001) basal spacing (Å) for cation saturated SWy-2 clays while exposed to atmospheric conditions (24°C), vacuum (10^{-3} Torr, 50°C), and CO_2 (90 bar, 50°C).

		atmosphere	Vacuum	CO_2
Clay	**Cation**	**1.0 bar**	**(10^{-3} Torr)**	**90 bar**
SWy-2	Cs	12.30	11.13	12.03
	NH_4	12.10	10.39	11.50
	Na	12.10	9.75	9.75

Pressurized MAS NMR

^{13}C

The ^{13}C MAS NMR resonances for the pure $scCO_2$ and $scCO_2$ plus Na^+ montmorillonite systems (**Figure 2**) are characterized by narrow center bands at ~124 ppm with full widths at half height (FWHH) of ~0.11 ppm. These narrow peaks reflect rapid, isotropic tumbling of CO_2 molecules in the supercritical fluid. There are also pairs of small spinning sidebands (SSBs). For pure $scCO_2$, these SSBs are likely associated with CO_2 either adsorbed to or being compressed on the rotor wall due to the centrifugal forces caused by the rotor rotation at ~3 kHz.

For Na-SWy-2-$scCO_2$, they are likely to arise from similar effects, given that their intensities are similar to those for $scCO_2$. Although they may also be associated with a small fraction of CO_2 weakly adsorbed to the exterior surfaces of clay particles.[55]

The center bands for the NH_4- and Cs-SWy-2 are also at ~124 ppm, demonstrating that the resonance comes from CO_2. However, the increased peak widths (FWHHs: ~0.31 ppm) indicate greater interaction of the CO_2 with solid surfaces and are consistent with greater restriction of CO_2 mobility. The SSB patterns are similar for the NH_4- and Cs-SWy-2 samples and are more intense with greater basal widths than for Na-SWy-2, showing four well resolved SSBs. The spans of the chemical shift anisotropy (CSA) for the NH_4- and Cs-SWy-2 are at least 160 ppm with a negative skew in each case. As discussed by Bowers et al.,[32] the SSBs are assigned to interlayer CO_2 molecules adsorbed in a 1WL-type (~12.5 Å) interlayer with the O-C-O molecular axes oriented parallel to the basal clay surface on average and experiencing rapid (>10^5 Hz) reorientation about an axis normal to the clay basal surface.[55]

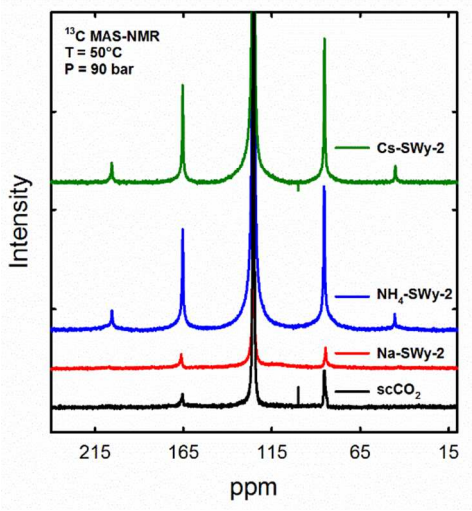

Figure 2. ^{13}C MAS NMR spectra of neat $scCO_2$, Na-SWy-2-$scCO_2$, NH_4-SWy-2-$scCO_2$, Cs-SWy-2-$scCO_2$ vertically expanded to highlight the spinning sideband patterns. Note that the Cs^+- and the NH_4^+- clays show evidence of interlayer-adsorbed CO_2 in the SSB patterns, whereas the Na^+ saturated clay shows no evidence of interlayer CO_2.

^{133}Cs

The ^{133}Cs NMR spectrum of Cs-SWy-2 at 50°C and 1 bar N_2 contains a broad center band at ~ 43 ppm and a well-developed SSB pattern (**Figure 3**). The broad peaks and broad spinning sideband manifold arise from strong paramagnetic coupling between $^{133}Cs^+$ and structural Fe in SWy-2,[56] consistent with the Cs^+ being close to the basal surfaces in collapsed interlayers.[53] These results are similar to those reported by Weiss et al.,[57] and others.[49, 52]

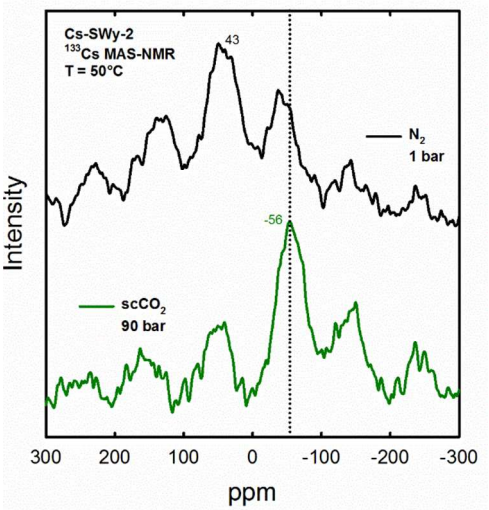

Figure 3. ^{133}Cs MAS NMR spectra of Cs-SWy-2 (top) and Cs-SWy-2-scCO$_2$, (bottom). Note the increase in area of the central peak due to CO$_2$-coordinated interlayer Cs$^+$ (-56 ppm).

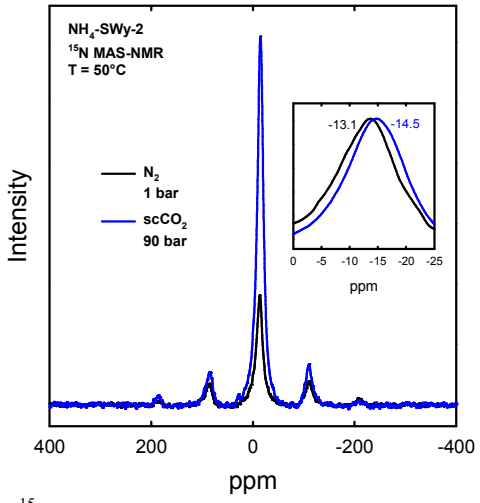

Figure 4. ^{15}N MAS NMR spectra of NH$_4$-SWy-2 before (bottom) and during (top) exposure to scCO$_2$, plotted on the same absolute intensity scale.

Following exposure to scCO$_2$, the ^{133}Cs centerband for Cs-SWy-2 shifts to -56 ppm but the strong SSB pattern remains. The full widths at half maximum of the centerband and spinning sidebands are very similar for both conditions (16 ± 9 ppm pre-CO$_2$ and 13 ± 5 ppm post-CO$_2$). However, the baseline flattens and the standard deviations of the FWHH decrease for the sample exposed to scCO$_2$. We interpret these changes to be due to reduced paramagnetic interaction with structural Fe in the clay as the distance between Cs and Fe increases with interlayer expansion. It is more difficult to comment on changes in the peak area since the magnitude of the quadropolar coupling and paramagnetic coupling are both changing as the coordination environment changes. The large change in the position of the ^{133}Cs center band is well correlated to the XRD data (**Table 1)** and previous studies of Cs-hectorite[32], and reflects a change in the coordination environment of Cs$^+$ due to some combination of interlayer expansion and Cs$^+$ solvation by CO$_2$.

^{15}N

The ^{15}N MAS NMR spectra of NH$_4$-SWy-2 show an appreciable increase in intensity, a small change in chemical shift, and little change in peak width after exposure to scCO$_2$ (6.0 ± 0.4 ppm without vs. 6.3 ± 0.6 ppm with) (**Figure 4**). With and without CO$_2$ the spectra contain one center band and four SSBs distributed symmetrically about the center band. In the presence of scCO$_2$, the central peak shifts from -13.1 ± 0.1 ppm to -14.5 ± 0.1 ppm, and the intensities of the central peak and SSBs increase dramatically, with the absolute intensity of the center band increasing by more than a factor of three during exposure to scCO$_2$. The increase in intensity reflects greater dynamic motion of the NH$_4^+$ cations due to interlayer expansion as CO$_2$ intercalates the clay, likely the result of more rapid NH$_4^+$ reorientation about the axes of molecular symmetry. As for the Cs-clay, we attribute the changes in the ^{15}N MAS NMR signal, which parallel the XRD results, to a combination of interlayer expansion and CO$_2$ solvation.

^{23}Na

The ^{23}Na MAS NMR spectrum of Na-SWy-2 at one bar (N$_2$) is dominated by a broad central peak and broad SSBs, consistent with Na$^+$ experiencing paramagnetic coupling to structural Fe (**Figure 5**).[56] In contrast to the Cs- and NH$_4$- samples, there is no significant change in the ^{23}Na signal after exposure to scCO$_2$, paralleling the XRD and ^{13}C NMR results that also show no changes during exposure to scCO$_2$. The better signal/noise ratio for the sample exposed to scCO$_2$ simply reflects longer acquisition times. Consequently, the ^{23}Na NMR spectrum clearly indicates that CO$_2$ does not intercalate dry Na-SWy-2. Accounting for the field-dependent quadrupolar shift of ^{23}Na, these results are very similar to those for dry Na-montmorillonite[58] and dry Na-hectorite.[59,60]

Molecular Dynamics Simulations

Molecular dynamics simulations were conducted in the grand canonical ensemble[61] for model Na$^+$-, Cs$^+$-, NH$_4^+$-montmorillonite (SWy-2) with imposed basal spacings using the RASPA software package.[62] The computed interlayer CO$_2$ contents and associated immersion energies of the SWy-2 clay systems vary significantly depending on the exchangeable cation (**Figure 6**). For Na-SWy-2, interlayer adsorption of CO$_2$ molecules begins only after the d(*00l*) basal spacing is substantially increased from the collapsed state at 9.5 ± 0.1 Å (vertical black line in **Figure 6**)[46, 48] to >10.7Å. Consequently, the immersion energy increases from *d*(001) = 9.5Å to 10.7Å, predicting that the

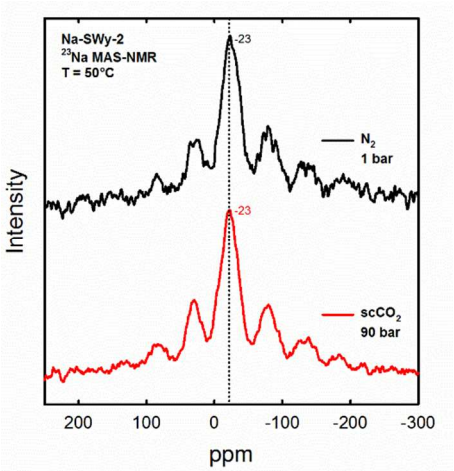

Figure 5. ^{23}Na MAS NMR of Na-SWy-2 (top) and Na-SWy-2-scCO$_2$ (bottom). Note the absence of any change in position or intensity of the central peak at – 23 ppm in the presence of scCO$_2$.

collapsed state is stable relative to the 1WL state and that there is a significant energetic barrier to CO_2 intercalation. This conclusion is consistent with previous molecular simulations by Makaremi et al.[40] Consequently, the modeling results are in accord with the experiments that showed no change in the basal spacing (**Table 1**) or ^{23}Na NMR signal upon exposure to $scCO_2$.

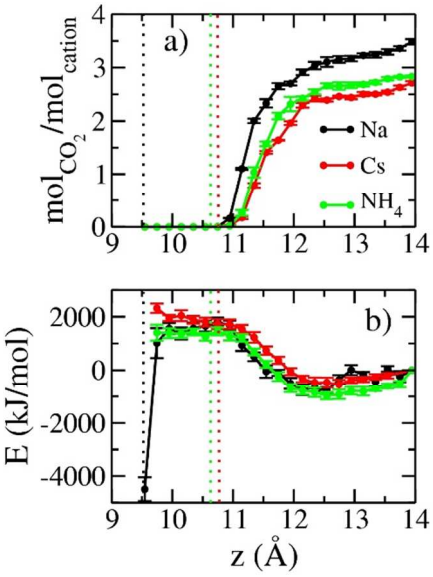

Figure 6. CO_2 content (a) and immersion energy of the system (b) as a function of basal spacing for SWy-2. The solid line at 9.5Å, 10.6Å, and 10.7Å indicate the collapsed basal spacing of Na^+ (black), NH_4^+ (green), and Cs^+ (red) clays, respectively. The error bars show the 95% confidence level. The reference state for the immersion energies is the 14.0Å basal spacing.

The computed *d*(001) value for fully collapsed Cs-SWy-2 (10.7 ± 0.2 Å; red vertical dotted line in **Figure 6a and b**) is similar to previous calculated values[48, 52-53], but slightly less than experimental values (**Table 1** and cited literature[18, 47-48]). The calculated *d*(001) value for fully collapsed NH_4-SWy-2 (10.6 ± 0.2 Å; delineated by the green vertical dotted lines in **Figure 6a and b**) is slightly larger than the experimentally determined value (10.39 Å). For both the Cs- and NH_4-systems the immersion energies of 1WL states (~12.5 Å) are significantly less than collapsed states, and there is no energy barrier to CO_2 intercalation (**Figure 6a**). For instance, the immersion energy decreases from ~1700 kJ/mol (10.7Å) to ~-500 kJ/mol (12.5Å) for Cs-SWy-2, while, the energy decreases from ~1400 kJ/mol (10.6Å) to ~-800 kJ/mol (12.5Å) with NH_4-SWy-2. Consequently, and in contrast to Na-SWy-2, the simulations indicate that CO_2 should readily enter the interlayer galleries of NH_4- and Cs-montmorillonites and form a stable expanded state (~12.5Å), in agreement with the XRD and NMR results.

The computed basal spacings of the 1WL states of NH_4- and Cs-SWy-2 at *d*(001) = ~12.5-12.6 Å are larger than the corresponding experimental values of 11.50 and 12.03 Å (**Table 1**). The models and experiments also showed somewhat different *d*(001) values for the fully collapsed clays (**Table 1**). In this regard, the calculated energy wells for the stable expanded states (around ~12.5Å) are broad and, consequently, the minimum energy *d*(001) values are not precisely known. Likewise, the simulations yielded energy plateaus for NH_4- and Cs-SWy-2 around the stable collapsed spacings (10.6Å – NH_4 and 10.7Å – Cs-SWy-2) and it is difficult to precisely determine the minimum energy *d*(001) in this region. In addition, the immersion energies show very little difference in magnitude (~1600 kJ/mol) between their collapsed state and at distances when CO_2 intercalation begins with Cs- and NH_4- SWy-2 (~10.9Å). It is also possible that the experiments did not reach equilibrium and record metastable states beyond the resolution of the simulations. We did not investigate energy versus *d*(001) behavior below 9.6 Å for the Na^+ clay.

Simulations indicate an equilibrium 1 WL (~12.5 Å) interlayer CO_2 content for NH_4-SWy-2 (2.61 mol CO_2/mol NH_4^+) that is slightly greater than for Cs-SWy-2 (2.40 mol CO_2/mol Cs^+) (**Figure 6a**) and that both are less than the value for the metastable 1WL state of the Na^+ clay (2.99 mol CO_2/mol Na^+). Recall, however, that CO_2 is not thermodynamically favored to intercalate the dry Na^+ clay; in this case, small concentrations of interlayer H_2O are required for CO_2 intercalation.[26, 30]

The energetic contribution from different interacting pairs involved during CO_2 intercalation with all 3 SWy-2 were examined to better understand the reason for the different behaviors of these clays. Figure 7 clearly illustrates that the primary cause for the large intercalation energy barrier for CO_2 with and the high stability of the collapsed state for Na-Swy-2 arises from the strong interaction of Na with the clay in contrast to the NH_4 and Cs-models. In particular, the difference in the Na/clay interaction energies between the collapsed state (9.5Å) and at the transition state for CO_2 intercalation (~10.8Å) is ~125 kJ/mol (Figure 7a). In contrast, the difference in interaction energies for NH_4/clay and Cs/Clay between their collapsed states (10.6Å - NH_4, 10.7Å - Cs) and their transition states for CO_2 intercalation (~10.9Å) is negli-

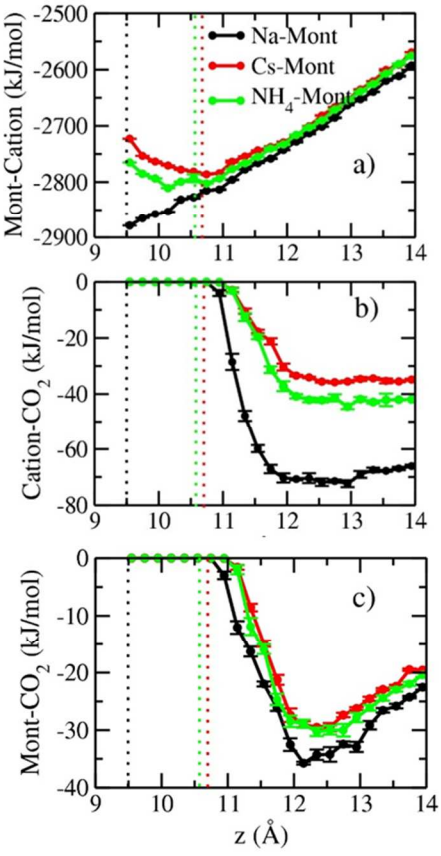

Figure 7. Variation in interaction energies between 3 different pairs. a) (SWy-2-Cation); b) Cation - CO_2; c) SWy-2-CO_2 as functions of interlayer spacing for Na-, Cs- and NH_4-SWy-2 at 323 K and 90 bar. Dotted vertical lines indicate respective collapsed interlayer distances for cations.

gible. At *d*(001) values > 10.7Å the interaction energies for Na/CO_2 are significantly larger than for Cs/CO_2 and NH_4/CO_2, consistent with the solvation energy trends reported in Figure 1. Further, CO_2/clay interaction energies are relatively similar for all the cations (Figure 7c). The small, but significantly more favorable CO_2/clay interaction for Na-SWy-2 (Figure 7c) might reflect the stronger CO_2/Na interaction energy (Figure 7b). Lastly, the sum of CO_2/Na and CO_2/clay interaction energies is always less favorable than the Na/clay interaction energy from the collapsed state up to the metastable state. Thus, the simulations indicate that it is the strong interaction of Na^+ with the clay that inhibits CO_2 intercalation and the relatively weak interaction of Cs and NH_4 with the clay that facilities CO_2 intercalation, in accord with experiment.

Quartz crystal microbalance (QCM) gas sorption measurements and discrete IR measurements (see Supplemental Information for details) were used to quantify the amount of interlayer CO_2 under the experimental conditions to compare to the calculated concentrations. While these experimental techniques cannot distinguish external from intercalated CO_2, the measurements help to validate the simulation results. Indeed, the IR intensity associated with the asymmetrical CO_2 band (**Figure 8**) trends with the simulations if we use the experimental *d*(001) values in **Table 1** to calculate the sorbed CO_2 concentrations from the simulation results plotted in **Figure 6a**. Similarly, these computed concentrations of CO_2 (0.0 mol CO_2/mol Na^+, 1.55 mol CO_2/mol NH_4^+, and 1.99 mol CO_2/mol Cs^+) trend well with our QCM measurements (0.5 mol CO_2/ mol Na^+, 1.74 mol CO_2/mol NH_4^+, and 3.66 mol CO_2/mol Cs^+). We suggest that the higher values for the QCM measured results are due to detection of both external and intercalated CO_2, whereas the simulations only quantify intercalated CO_2.

Is there a stable expanded state for Na-clay?

The immersion energy plots for Na-SWy-2 (**Figure 6b**) indicate that the collapsed basal spacing (9.5Å) is the most stable state, with energy minimum of ~-4500 kJ/mol when compared to -700

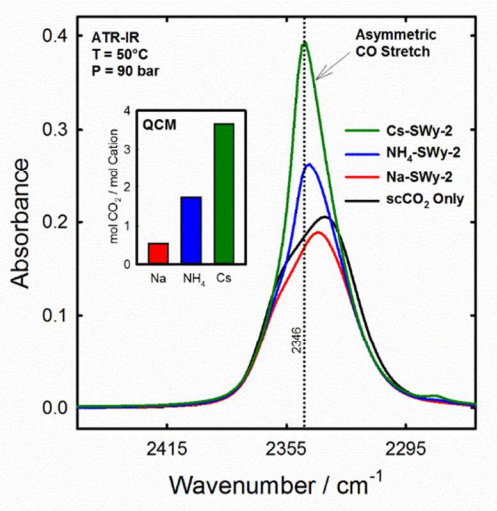

Figure 8. IR spectra in the asymmetric CO stretching of CO_2 in the presence of Na-, Cs-, and NH_4-SWy-2 at 90 bar and 50°C. Also shown for comparison is that spectrum of bulk $scCO_2$ under the same conditions.

kJ/mol hypothetical metastable state at ~12.5 Å, in agreement with Makaremi et al.,[20] and our own calculations. To verify the computational results, we performed a series of high pressure IR experiments using an initially hydrated 1WL Na-SWy-2 , a composition known to facilitate CO_2 intercalation (see SI),[26] and then systematically dehydrated the clay. The hydrated clay was first exposed to $scCO_2$ at 90 bars and 50°C and then cycled between 90 and 180 bars at constant temperature, where the fluid was leaked out of the cell on each down-pressure leg of the cycle and fresh CO_2 injected on every upward-pressure leg. The results show that as the clay dehydrated, eventually to the collapsed state (9.67 Å), intercalated CO_2 was systematically and nearly completely expelled from the interlayer region. We then performed a similar experiment except the clay was cycled between $scCO_2$ at 90 bars and 50°C, and liquid CO_2 at 90 bars and 25°C, with CO_2+H_2O leaked on the upward-temperature leg of the cycle and fresh $ChyO_2$ injected on every down-pressure leg. The results were the same: As the clay dehydrated, CO_2 was expelled from the interlayer region. Consequently, these experiments are in agreement with our GCMD calculations and the computed results of Makaremi et al.,[40] showing that the collapsed state of Na-montmorillonite is the stable state in equilibrium with dry $scCO_2$.

CONCLUSION and IMPLICATIONS

Experiments and complementary GCMD simulations for Na-, NH_4- and Cs-SWy-2 exposed to dry $scCO_2$ at 50°C and 90 bars reveal that because this weakly polar solvent does not strongly solvate the interlayer cations the tendency to intercalate and swell is controlled instead by the strength of the cation interaction with the aluminosilicate sheets. The stable state of the Na-clay is the fully collapsed interlayer region with no intercalated CO_2. Further, the Na-clay exhibits a large energy barrier for CO_2 intercalation. In contrast, the stable state of the NH_4- and Cs-clay is an expanded, 1WL-like state, containing substantial interlayer CO_2, coupled with little to no energy barrier for CO_2 diffusion into the interlayer region. The combination of experiment and theory demonstrates, for the first time, that it is the cation-clay interaction that determines the extent of interlayer expansion and absorption of relatively low dielectric volatiles by swelling clays. This is in contrast to cation-H_2O interactions, where the hydration energy of the cation dominates interlayer expansion behavior. In addition to the cationic radius to charge characteristics, this also suggests that clay swelling in weakly polar solvents will be more sensitive to the layer charge and its distribution between tetrahedral and octahedral sites compared to H_2O-containing systems.

EXPERIMENTAL SECTION

The smectite used in our studies, Wyoming bentonite (SWy-2) was obtained from the Source Clays Repository of the Clay Mineral Society (Purdue University, www.agry.purdue.edu/cjohnston/sourceclays). The as-received SWy-2 clay was processed using the procedures of Loring et al.,[26] and saturated with Na^+, NH_4^+, or Cs^+. For the XRD, dilute clay suspensions were prepared by suspending the cation saturated clays in water. NMR experiments required dry powders, which were obtained by drying clay suspensions on glass slides at room temperature. The resulting clay films were scraped off with a razor blade and placed into glass vials. The clays were characterized by XRD while either under vacuum or during exposure to CO_2 (3.45 or 90 bar) at 50°C using a high pressure and temperature X-ray diffraction technique described previously.[13, 55] Initially, measured aliquots of dilute clay suspensions were pipetted onto a beryllium post, each occupying a circular area with an approximate diameter of 2-3 mm. Each clay mount was allowed to air dry to produce a thin preferentially oriented clay film. The alignment process consisted of placing the beryllium post onto the XYZ stage and with the aid of the laser alignment system, manipulating the stage to expose only one clay film at a time to the XRD beam. Once the coordinates were established, the pressurized reactor was assembled, mounted into the instrument, and heated to 50°C. Subsequent exposure to vacuum for 30 minutes removed most of the water from the clays. Pressurization with

CO_2 was accomplished through an ISCO pump connected directly to the reactor. Patterns were collected using a Bruker D8 Discover XRD instrument with a rotating Cu anode (CuK alpha =1.5418 Å), programmable XYZ customized stage, and a Vantec 500 detector set at a sample-to-detector distance of 15 cm. This instrument, operated at 50 kV and 24 mA, is capable of producing an intensely focused 0.5 mm beam. The resulting XRD patterns had an acquisition time of 300 seconds, were integrated over a range of 4-45° 2 θ, and subsequently analyzed with the MDI JADE® XRD software package (Materials Data Inc, Livermore, Ca, 64550) to obtain peak positions.

^{13}C, ^{23}Na, ^{15}N, and ^{133}Cs MAS NMR spectra were collected under pressurized conditions at 90 bar CO_2 and 50°C after first exposing each sample to dry nitrogen at 50°C and 1 bar. The NMR spectra were acquired at an H_0 magnetic field of 7.0 T with a Varian VNMRS console. The solid-state probe was a 7.5 mm HXMAS Chemagnetics style probe with a ceramic housing. The zirconia rotors were altered and fitted with gas tight valves for pressurization. The ^{13}C MAS NMR data were acquired using a standard Bloch-decay pulse sequence with a pi/2 pulse width of 7.75 microseconds to obtain 700 transients. These data involved a spectral width of 50 kHz, a number of points per transient of 30k, and a spin rate of approximately 3 kHz. The ^{133}Cs data were referenced to a 0.1 M solution of CsCl using a secondary standard of CsCl (s). Spectra represent Bloch-decay data acquired using a spectral width of ~200 kHz, 18k-28k transients, a spin rate of 3.5 kHz, π/2 pulse width of 8 μs, and a pulse delay of 0.5 s. The ^{15}N data were also acquired with a Bloch-decay pules sequence with a π/2 pulse width of 7 μs, a spectral width of 100 kHz, pulse delay of 1 s, and a spin rate of 3 kHz to obtain 5000 transients. The ^{23}Na data were acquired using a standard quadrupolar echo sequence to improve flatness of the baseline. These data sets involved acquiring ~5k transients for the low pressure sample and 10k transients for the sample exposed to $scCO_2$. Both used a MAS frequency of 4 kHz, spectral width of 100 kHz, pulse delay of 0.5 s, and a π/2 pulse width of 4.5 μs. All NMR data were processed using iNMR, a commercial program by MestReC (http://www.inmr.net), and all NMR results were iteratively fit using Abscissa, a freeware app written by Rudiger Bruhl (http://rbruehl.macbay.de). For the ^{13}C MAS NMR, the time domain spectra were zero filled to a Fourier number (FN) of 32k points and given 5 Hz of exponential apodization prior to the Fourier transform (FT). For the ^{133}Cs MAS NMR spectra, the data were zero filled to a FN of 64k points, the first three points were removed, and 200 Hz of exponential apodization applied before the FT. For the ^{23}Na MAS NMR spectra data were left shifted by one data point, zero filled to a FN of 32k points, and received 200 Hz of exponential apodization prior to the FT. The ^{15}N NMR spectra used a zero fill to an FN of 16k points, a left shift of four data points, and 50 Hz of exponential apodization before the FT. In almost all cases a standard baseline correction was performed to flatten the baseline. All peak fits were performed by iteratively fitting the data set to Lorentzian lineshapes.

Molecular Dynamics Simulations

Molecular dynamics simulations were conducted in the grand canonical ensemble (GCMD)[61] for Na^+-, Cs^+-, NH_4^+-montmorillonite. The SWy-2 model was obtained from Ngouana and Kalinichev[48] and has a structural formula of $M^+_{0.75}(Si_{7.75}Al_{0.25})(Al_{3.5}Mg_{0.5})O_{20}(OH)_4$. The distributions of the octahedral and tetrahedral isomorphic substitutions follow a disordered pattern in accordance with Loewenstein's rule.[63]

The simulation supercells for all the systems consist of 32 crystallographic unit cells of montmorillonite (4 x 4 x 2) and encompass two interlayers with surface areas of 740.2Å^2. The large surface areas are necessary to overcome finite size effects in the simulated models. The basal spacings were varied from 9.5Å to 14.0Å at steps of 0.2Å. Both interlayer galleries were constrained to have same dimensions, which were held constant throughout the simulation runs. All of the cations were initially placed at the midplane of the interlayers. The T-O-T layers were allowed to move only laterally, parallel to the basal surface, without disrupting the structure. Such translational movement is essential, because the *x-y* displacement of the minimum energy interlayer structure depends on the cation and the number of intercalated fluid molecules, here CO_2, as has been reported in previous studies.[37]

The GCMD simulations were performed with the RASPA[62] simulation package. GCMD is a hybrid method which involves coupling of Monte Carlo and MD methods. In the grand canonical ensemble system temperature, system volume, and the chemical potential of the fluid molecules are fixed, but the number of adsorbed molecules fluctuates. This is achieved by sampling insertion and deletion of fluid molecules with equal probability at every MD step. The interatomic interactions for the smectite T-O-T layers and cations were obtained using the *CLAYFF* force field, which is used widely in clay simulations.[48, 53,64] The CO_2 molecules were represented with the rigid EPM2 model.[35] The parameters for the rigidly held NH_4^+ ions were obtained from the literature.[65] All the GCMD simulations were performed at T=323 K and P=90 bars for 12 ns to reach equilibration followed by another 8 ns for the production run. The MD time step was 1 fs. Periodic boundary conditions in three dimensions were employed with a cutoff of 9.0 Å for short range non-electrostatic interactions. Ewald summation was used for computing long-range electrostatic interactions with an accuracy of 10^{-6}. A Nosé-Hoover thermostat were used to control the temperature.[66] Fugacities required to run the simulation were obtained using the Peng-Robinson equation of state.[67] The critical temperature, critical pressure and acentric factor used to automatically compute the fugacity in RASPA using the equation of state.[67] The computed fugacity coefficient of CO_2 molecules at 323K and 90 bar corresponds to 0.654. The adsorption isotherms and related immersion energies were calculated using the data from the last 2 ns of the equilibrium trajectory. The reported mean values are obtained using statistical averages over 5 equal time blocks of 400 ps each. The use of immersion energies to investigate the equilibrium states of smectite systems has been discussed previously for water adsorption[52-53] and is extended here to CO_2.

ASSOCIATED CONTENT

Supporting Information. Methods section detailing the infrared and quartz crystal microbalance techniques; X-ray diffraction tracings of clays exposed to vacuum and pressurized CO_2; electronic structure calculations of the solvation energy of the cations shown in Figure 1. This material is available free of charge via the Internet at http://pubs.acs.org.

AUTHOR INFORMATION

Corresponding Authors

HT Schaef, todd.schaef@pnnl.gov
ES Ilton, eugene.ilton@pnnl.gov
JS Loring, john.loring@pnnl.gov

Author Contributions

The manuscript was written through contributions of all authors. All authors have given approval to the final version of the manuscript.

ACKNOWLEDGMENT

This material is based upon work supported by the U.S. Department of Energy (DOE), Office of Science, Office of Basic Energy Sciences (BES), Chemical Sciences, Geosciences, and Biosciences Division through its Geosciences program at Pacific Northwest National Laboratory (PNNL) (JSL, ESI, KST, DAD, KMR), and through its university grants DE-FG02-10ER16128 and DE-FG02-08ER15929 (GMB, NL, AOY, RJK). DAD also thanks the Robert Ramsay Fund at the University of Alabama for support. It is also based upon work supported by the DOE Office of Fossil Energy at PNNL through the National Energy Technology Laboratory, Morgantown, West Virginia (HTS, BPM). SDB and DWH collected the NMR data at the Environmental Molecular Science Laboratory (EMSL), a DOE Office of Science User Facility sponsored by the Office of Biological and Environmental Research and located at PNNL. The authors would like to thank Dr. Sebastien Kerisit for insightful comments.

REFERENCES

(1) Kuila, U.; McCarty, D. K.; Derkowski, A.; Fischer, T. B.; Topor, T.; Prasad, M. Nano-Scale Texture and Porosity of Organic Matter and Clay Minerals in Organic-Rich Mudrocks. *Fuel* **2014,** *135*, 359-373.

(2) Kuila, U.; Prasad, M. Specific Surface Area and Pore-Size Distribution in Clays and Shales. *Geophys. Prospect.* **2013,** *61* (2), 341-362.

(3) Ross, D. J. K.; Bustin, R. M. The Importance of Shale Composition and Pore Structure Upon Gas Storage Potential of Shale Gas Reservoirs. *Mar. Pet. Geol.* **2009,** *26* (6), 916-927.

(4) Busch, A.; Bertier, P.; Gensterblum, Y.; Rother, G.; Spiers, C. J.; Zhang, M.; Wentinck, H. M. On Sorption and Swelling of CO_2 in Clays. *Geomechanics and Geophysics for Geo-Energy and Geo-Resources* **2016,** *2* (2), 111-130.

(5) Josh, M.; Esteban, L.; Delle Piane, C.; Sarout, J.; Dewhurst, D. N.; Clennell, M. B. Laboratory Characterisation of Shale Properties. *J. Pet. Sci. Eng.* **2012,** *88-89*, 107-124.

(6) Gaus, I. Role and Impact of CO_2-rock Interactions During CO_2 Storage in Sedimentary Rocks. *Int. J. Greenhouse Gas Control* **2010,** *4* (1), 73-89.

(7) Middleton, R. S.; Gupta, R.; Hyman, J. D.; Viswanathan, H. S. The Shale Gas Revolution: Barriers, Sustainability, and emerging Opportunities. *Appl. Energy* **2017,** *199*, 88-95.

(8) Liu, S. Y.; Yan, Z. L.; Fu, L. J.; Yang, H. M. Hierarchical Nano-Activated Silica Nanosheets for Thermal Energy Storage. *Sol. Energy Mater. Sol. Cells* **2017,** *167*, 140-149.

(9) Guo, Z. Q.; Li, Y.; Zhang, S. W.; Niu, H. H.; Chen, Z. S.; Xu, J. Z. Enhanced Sorption of Radiocobalt from Water by Bi(III) Modified Montmorillonite: A Novel Adsorbent. *J. Hazard. Mater.* **2011,** *192* (1), 168-175.

(10) Yang, R. T.; Baksh, M. S. A. Pillared Clays as a New Class of Sorbents for Gas Separation *AIChE Journal* **1991,** *37* (5), 679-686.

(11) De Pourcq, K.; Ayora, C.; Garcia-Gutierrez, M.; Missana, T.; Carrera, J. A Clay Permeable Reactive Barrier to Remove Cs-137 from Groundwater: Column Experiments. *J. Environ. Radioact.* **2015,** *149*, 36-42.

(12) Segad, M.; Jonsson, B.; Akesson, T.; Cabane, B. Ca/Na Montmorillonite: Structure, Forces and Swelling Properties. *Langmuir* **2010,** *26* (8), 5782-5790.

(13) Schaef, H. T.; Ilton, E. S.; Qafoku, O.; Martin, P. F.; Felmy, A. R.; Rosso, K. M. In situ XRD Study of Ca^{2+} Saturated Montmorillonite (STX-1) Exposed to Anhydrous and Wet Supercritical Carbon Dioxide. *Int. J. Greenhouse Gas Control* **2012**, 220-229.

(14) Ferrage, E.; Lanson, B.; Sakharov, B. A.; Drits, V. A. Investigation of Smectite Hydration Properties by Modeling Experimental X-ray Diffraction Patterns: Part I. Montmorillonite Hydration Properties. *Am. Mineral.* **2005,** *90* (8-9), 1358-1374.

(15) Busch, A.; Alles, S.; Gensterblum, Y.; Prinz, D.; Dewhurst, D. N.; Raven, M. D.; Stanjek, H.; Krooss, B. M. Carbon Dioxide Storage Potential of Shales. *Int. J. Greenhouse Gas Control* **2008,** *2* (3), 297-308.

(16) Sun, L. L.; Hirvi, J. T.; Schatz, T.; Kasa, S.; Pakkanen, T. A. Estimation of Montmorillonite Swelling Pressure: A Molecular Dynamics Approach. *J. Phys. Chem. C* **2015,** *119* (34), 19863-19868.

(17) Pei, P.; Ling, K. G.; He, J.; Liu, Z. Z. Shale Gas Reservoir Treatment by a CO_2-Based Technology. *J. Nat. Gas Sci. Eng.* **2015,** *26*, 1595-1606.

(18) Berend, I.; Cases, J. M.; Francois, M.; Uriot, J. P.; Michot, L.; Masion, A.; Thomas, F. Mechanism of Adsorption and Desorption of Water-Vapor by Homoionic Montmorillonites 2. The Li^+, Na^+, K^+, Rb^+, and Cs^+-Exchanged Forms. *Clays Clay Miner.* **1995,** *43* (3), 324-336.

(19) Cases, J. M.; Berend, I.; Besson, G.; Francois, M.; Uriot, J. P.; Thomas, F.; Poirier, J. E. Mechanism of Adsorption and Desorption of Water-Vapor by Homoionic Montmorilonite. 1. The Sodium-Exchanged Form *Langmuir* **1992,** *8* (11), 2730-2739.

(20) Cases, J. M.; Berend, I.; Francois, M.; Uriot, J. P.; Michot, L. J.; Thomas, F. Mechanism of Adsorption and Desorption of Water vapor by Homoionic Montmorillonite .3. The Mg^{2+}, Ca^{2+}, Sr^{2+} and Ba^{2+} Exchanged Forms. *Clays Clay Miner.* **1997,** *45* (1), 8-22.

(21) Whitley, H. D.; Smith, D. E. Free Energy, Energy, and Entropy of Swelling in Cs-, Na-, and Sr-Montmorillonite Clays. *J. Chem. Phys.* **2004,** *120* (11), 5387-5395.

(22) Teich-McGoldrick, S. L.; Greathouse, J. A.; Jove-Colon, C. F.; Cygan, R. T. Swelling Properties of Montmorillonite and Beidellite Clay Minerals from Molecular Simulation: Comparison of Temperature, Interlayer Cation, and Charge Location Effects. *J. Phys. Chem. C* **2015,** *119* (36), 20880-20891.

(23) Loring, J. S.; Schaef, H. T.; Turcu, R. V. F.; Thompson, C. J.; Miller, Q. R. S.; Martin, P. F.; Hu, J. Z.; Hoyt, D. W.; Qafoku, O.; Ilton, E. S.; Felmy, A. R.; Rosso, K. M. In Situ Molecular Spectroscopic Evidence for CO_2 Intercalation into Montmorillonite in Supercritical Carbon Dioxide. *Langmuir* **2012,** *28* (18), 7125-7128.

(24) Loring, J. S.; Schaef, H. T.; Thompson, C. J.; Turcu, R. V.; Miller, Q. R.; Chen, J.; Hu, J.; Hoyt, D. W.; Martin, P. F.; Ilton, E. S.; Felmy, A. R.; Rosso, K. M. Clay Hydration/dehydration in Dry to Water-saturated Supercritical CO_2: Implications for Caprock Integrity. *Energy Procedia* **2013,** *37* (0), 5443-5448.

(25) Ilton, E. S.; Schaef, H. T.; Qafoku, O.; Rosso, K. M.; Felmy, A. R. In Situ X-ray Diffraction Study of Na+ Saturated Montmorillonite Exposed to Variably Wet Super Critical CO_2. *Environ. Sci. Technol.* **2012,** *46* (7), 4241-4248.

(26) Loring, J. S.; Ilton, E. S.; Chen, J.; Thompson, C. J.; Martin, P. F.; Bénézeth, P.; Rosso, K. M.; Felmy, A. R.; Schaef, H. T. In Situ Study of CO_2 and H_2O Partitioning Between Na–Montmorillonite and Variably Wet Supercritical Carbon Dioxide. *Langmuir* **2014,** *30* (21), 6120-6128.

(27) Giesting, P.; Guggenheim, S.; van Groos, A. F. K.; Busch, A. X-ray Diffraction Study of K- and Ca-Exchanged Montmorillonites in CO_2 Atmospheres. *Environ. Sci. Technol.* **2012,** *46* (10), 5623-5630.

(28) Giesting, P.; Guggenheim, S.; van Groos, A. F. K.; Busch, A. Interaction of Carbon Dioxide with Na-Exchanged Montmorillonite at Pressures to 640 Bars: Implications for CO_2 Sequestration. *Int. J. Greenhouse Gas Control* **2012,** *8*, 73-81.

(29) Rother, G.; Ilton, E. S.; Wallacher, D.; Hauss, T.; Schaef, H. T.; Qafoku, O.; Rosso, K. M.; Felmy, A. R.; Krukowski, E. G.; Stack, A. G.; Grimm, N.; Bodnar, R. J. CO_2 Sorption to Subsingle Hydration Layer Montmorillonite Clay Studied by Excess Sorption and Neutron Diffraction Measurements. *Environ. Sci. Technol.* **2013,** *47* (1), 205-211.

(30) Schaef, H. T.; Loring, J. S.; Glezakou, V.-A.; Miller, Q. R. S.; Chen, J.; Owen, A. T.; Lee, M.-S.; Ilton, E. S.; Felmy, A. R.; McGrail, B. P.; Thompson, C. J. Competitive Sorption of CO_2 and H_2O in 2:1 Layer Phyllosilicates. *Geochim. Cosmochim. Acta* **2015,** *161*, 248-257.

(31) Kadoura, A.; Narayanan Nair, A. K.; Sun, S. Molecular Simulation Study of Montmorillonite in Contact with Variably Wet Supercritical Carbon Dioxide. *J. Phys. Chem. C* **2017,** *121* (11), 6199-6208.

(32) Rao, Q.; Leng, Y. Molecular Understanding of CO_2 and H_2O in a Montmorillonite Clay Interlayer under CO_2 Geological Sequestration Conditions. *J. Phys. Chem. C* **2016,** *120* (5), 2642-2654.

(33) Sena, M. M.; Morrow, C. P.; Kirkpatrick, R. J.; Krishnan, M. Supercritical Carbon Dioxide at Smectite Mineral–Water Interfaces: Molecular Dynamics and Adaptive Biasing Force Investigation of CO_2/H_2O Mixtures Nanoconfined in Na-Montmorillonite. *Chem. Mater.* **2015,** *27* (20), 6946-6959.

(34) Criscenti, L. J.; Cygan, R. T. Molecular Simulations of Carbon Dioxide and Water: Cation Solvation. *Environ. Sci. Technol.* **2013,** *47* (1), 87-94.

(35) Cygan, R. T.; Romanov, V. N.; Myshakin, E. M. Molecular Simulation of Carbon Dioxide Capture by Montmorillonite Using an Accurate and Flexible Force Field. *J. Phys. Chem. C* **2012,** *116* (24), 13079-13091.

(36) Myshakin, E. M.; Saidi, W. A.; Romanov, V. N.; Cygan, R. T.; Jordan, K. D. Molecular Dynamics Simulations of Carbon Dioxide Intercalation in Hydrated Na-Montmorillonite. *J. Phys. Chem. C* **2013,** *117* (21), 11028-11039.

(37) Botan, A.; Rotenberg, B.; Marry, V.; Turq, P.; Noetinger, B. t. Carbon Dioxide in Montmorillonite Clay Hydrates: Thermodynamics, Structure, and Transport from Molecular Simulation. *J. Phys. Chem. C* **2010,** *114* (35), 14962-14969.

(38) Zhang, W.; Hu, H.; Li, X.; Fang, Z. Interplay of Montmorillonite–H_2O–$scCO_2$ System Between Mechanical Behavior and Adsorption: Molecular Dynamics. *J. Phys. Chem. C* **2015,** *119* (38), 21959-21968.

(39) Krishnan, M.; Saharay, M.; Kirkpatrick, R. J. Molecular Dynamics Modeling of CO_2 and Poly(ethylene glycol) in Montmorillonite: The Structure of Clay-Polymer Composites and the Incorporation of CO_2. *J. Phys. Chem. C* **2013,** *117* (40), 20592-20609.

(40) Makaremi, M.; Jordan, K. D.; Guthrie, G. D.; Myshakin, E. M. Multiphase Monte Carlo and Molecular Dynamics Simulations of Water and CO_2 Intercalation in Montmorillonite and Beidellite. *J. Phys. Chem. C* **2015,** *119* (27), 15112-15124.

(41) Myshakin, E. M.; Makaremi, M.; Romanov, V. N.; Jordan, K. D.; Guthrie, G. D. Molecular Dynamics Simulations of Turbostratic Dry and Hydrated Montmorillonite with Intercalated Carbon Dioxide. *J. Phys. Chem. A* **2014,** *118* (35), 7454-7468.

(42) Lee, M.-S.; McGrail, B. P.; Glezakou, V.-A. Microstructural Response of Variably Hydrated Ca-rich Montmorillonite to Supercritical CO_2. *Environ. Sci. Technol.* **2014,** *48* (15), 8612-8619.

(43) Sidey, V. On the Effective Ionic Radii for Ammonium. *Acta Crystallogr., Sect. B: Struct. Sci.* **2016,** *72*, 626-633.

(44) Emsley, J. *The Elements*, 2nd ed.; Clarendon Press: Oxford, 1991

(45) Cruz-Guzmán, M.; Celis, R.; Hermosín, M. C.; Cornejo, J. Adsorption of the Herbicide Simazine by Montmorillonite Modified with Natural Organic Cations. *Environ. Sci. Technol.* **2004,** *38* (1), 180-186.

(46) Morrow, C. P.; Yazaydin, A. O.; Krishnan, M.; Bowers, G. M.; Kalinichev, A. G.; Kirkpatrick, R. J. Structure, Energetics, and Dynamics of Smectite Clay Interlayer Hydration: Molecular Dynamics and Metadynamics Investigation of Na-Hectorite. *J. Phys. Chem. C* **2013,** *117* (10), 5172-5187.

(47) Gautier, M.; Muller, F.; Le Forestier, L.; Beny, J. M.; Guegan, R. NH4-Smectite: Characterization, Hydration Properties and Hydro Mechanical Behaviour. *Appl. Clay Sci.* **2010,** *49* (3), 247-254.

(48) Ngouana, B. F.; Kalinichev, A. G. Structural Arrangements of Isomorphic Substitutions in Smectites: Molecular Simulation of the Swelling Properties, Inter layer Structure, and Dynamics of Hydrated Cs-Montmorillonite Revisited with New Clay Models. *J. Phys. Chem. C* **2014,** *118* (24), 12758-12773.

(49) Kosakowski, G.; Churakov, S. V.; Thoenen, T. Diffusion of Na and Cs in Montmorillonite. *Clays Clay Miner.* **2008,** *56* (2), 190-206.

(50) Shannon, R. D. Revised Effective Ionic-Radii and Systematic Studies of Interatiomic Distances in Halides and Chalcogenides. *Acta Crystallogr. Sect. A* **1976,** *32* (SEP1), 751-767.

(51) Masterton, W. L.; Bolocofsky, D.; Lee, T. P. Ionic Radii from Scaled Particle Theory of Salt Effect. *J. Phys. Chem.* **1971,** *75* (18), 2809-2815.

(52) Smith, D. E. Molecular Computer Simulations of the Swelling properties and Interlayer Structure of Cesium Montmorillonite. *Langmuir* **1998,** *14* (20), 5959-5967.
(53) Loganathan, N.; Yazaydin, A. O.; Bowers, G. M.; Kalinichev, A. G.; Kirkpatrick, R. J. Structure, Energetics, and Dynamics of Cs^+ and H_2O in Hectorite: Molecular Dynamics Simulations with an Unconstrained Substrate Surface. *J. Phys. Chem. C* **2016,** *120* (19), 10298-10310.
(54) Vivaldi, J. L. M.; Vilchez, F. G.; Hernaiz, M.; Castro, B. d.; Gallego, M. R. The Thermal Decomposition of NH_4 Montmorillonites. Part 1. *Mineralogical Society of Great Britain and Ireland* **1959**, 81-87.
(55) Bowers, G. M.; Schaef, H. T.; Loring, J. S.; Hoyt, D. W.; Burton, S. D.; Walter, E. D.; Kirkpatrick, R. J. Role of Cations in CO_2 Adsorption, Dynamics, and Hydration in Smectite Clays under in Situ Supercritical CO_2 Conditions. *J. Phys. Chem. C* **2017,** *121* (1), 577-592.
(56) Bank, S.; Bank, J. F.; Ellis, P. D. Solid-State ^{113}Cd Nuclear Magnetic-Resonance Study of Exchanged Montmorillonites. *J. Phys. Chem.* **1989,** *93* (12), 4847-4855.
(57) Weiss, C. A.; Kirkpatrick, R. J.; Altaner, S. P. The Structural Environments of Cations Adsorbed Onto Clays ^{133}Cs Variable Temperature MAS NMR Spectroscopic Study of Hectorite *Geochim. Cosmochim. Acta* **1990,** *54* (6), 1655-1669.
(58) Reinholdt, M. X.; Kirkpatrick, R. J.; Pinnavaia, T. J. Montmorillonite-poly(ethylene oxide) Nanocomposites: Interlayer Alkali Metal Behavior. *J. Phys. Chem. B* **2005,** *109* (34), 16296-16303.
(59) Bowers, G. M.; Singer, J. W.; Bish, D. L.; Kirkpatrick, R. J. Alkali Metal and H_2O Dynamics at the Smectite/Water Interface. *J. Phys. Chem. C* **2011,** *115* (47), 23395-23407.
(60) Aranda, P.; Ruizhitzky, E. Poly(Ethylene Oxide)-Silicate Intercalation materials *Chem. Mater.* **1992,** *4* (6), 1395-1403.
(61) Boinepalli, S.; Attard, P. Grand Canonical Molecular Dynamics. *J. Chem. Phys.* **2003,** *119* (24), 12769-12775.
(62) Dubbeldam, D.; Calero, S.; Ellis, D. E.; Snurr, R. Q. RASPA: Molecular Simulation Software for Adsorption and Diffusion in Flexible Nanoporous Materials. *Mol. Simul.* **2016,** *42* (2), 81-101.
(63) Loewenstein, W. The Distribution of Aluminum in the Tetrahedra of Silicates and Aluminates. *Am. Mineral.* **1954,** *39* (1-2), 92-96.
(64) Cygan, R. T.; Liang, J. J.; Kalinichev, A. G. Molecular Models of Hydroxide, Oxyhydroxide, and Clay Phases and the Development of a General Force Field. *J. Phys. Chem. B* **2004,** *108* (4), 1255-1266.
(65) Loganathan, N.; Kalinichev, A. G. On the Hydrogen Bonding Structure at the Aqueous Interface of Ammonium-Substituted Mica: A Molecular Dynamics Simulation. *Zeitschrift Fur Naturforschung Section a-a Journal of Physical Sciences* **2013,** *68* (1-2), 91-100.
(66) Shinoda, W.; Shiga, M.; Mikami, M. Rapid Estimation of Elastic Constants by Molecular Dynamics Simulation Under Constant Stress. *Phys. Rev. B* **2004,** *69* (13).
(67) Peng, D.; Robinson, D. B. New 2-constant Equeation of State *Ind. Eng. Chem. Fundam.* **1976,** *15* (1), 59-64.

TOC